Euclid: the potential of slitless infrared spectroscopy: a $z = 5.4$ quasar and new ultracool dwarfs

E. Bañados [ID],[1]★ V. Le Brun,[2]† S. Belladitta,[1,3] I. Momcheva,[1] D. Stern,[4] J. Wolf,[1] M. Ezziati,[2] D. J. Mortlock [ID],[5,6] A. Humphrey,[7,8] R. L. Smart,[9,10] S. L. Casewell,[11] A. Pérez-Garrido,[12] B. Goldman,[13,14] E. L. Martín,[15,16] A. Mohandasan,[17] C. Reylé,[17] C. Dominguez-Tagle,[15,16] Y. Copin,[18] E. Lusso,[19,20] Y. Matsuoka,[21] K. McCarthy,[4] F. Ricci,[22,23] H.-W. Rix,[1] H. J. A. Rottgering,[24] J.-T. Schindler,[25] J. R. Weaver,[26] A. Allaoui,[2] T. Bedrine,[2] M. Castellano,[23] P.-Y. Chabaud,[2] G. Daste,[2] F. Dufresne,[2] J. Gracia-Carpio,[27] M. Kümmel,[28] M. Moresco,[3,29] M. Scodeggio,[30] C. Surace,[2] D. Vibert,[2] A. Balestra,[31] A. Bonnefoi,[2] A. Caillat,[2] F. Cogato,[3,29] A. Costille,[2] S. Dusini,[32] S. Ferriol,[18] E. Franceschi,[3] W. Gillard,[33] K. Jahnke,[1] D. Le Mignant,[2] S. Ligori,[9] E. Medinaceli,[3] G. Morgante,[3] F. Passalacqua,[32,34] K. Paterson,[1] S. Pires,[35] C. Sirignano,[32,34] I. T. Andika,[36,37] H. Atek,[38] D. Barrado,[39] S. Bisogni,[30] C. J. Conselice,[40] H. Dannerbauer,[41] R. Decarli,[3] H. Dole,[42] T. Dupuy,[43] A. Feltre,[19] S. Fotopoulou,[44] B. Gillis,[43] X. Lopez Lopez,[3,29] M. Onoue,[45,46] G. Rodighiero,[31,34] N. Sedighi,[15,16] F. Shankar,[47] M. Siudek,[41,48] L. Spinoglio,[49] D. Vergani,[3] G. Vietri,[30] F. Walter,[1] G. Zamorani,[3] M. R. Zapatero Osorio,[39] J.-Y. Zhang,[15,16] M. Bethermin,[14] N. Aghanim,[42] B. Altieri,[50] A. Amara,[51] S. Andreon,[52] C. Baccigalupi,[53,54,55,56] M. Baldi,[3,57,58] S. Bardelli,[3] A. Basset,[59] P. Battaglia,[3] A. Biviano,[53,54] A. Bonchi,[60] D. Bonino,[9] E. Branchini,[52,61,62] M. Brescia,[63,64] J. Brinchmann,[7,65] S. Camera,[9,66,67] V. Capobianco,[9] C. Carbone,[30] J. Carretero,[68,69] S. Casas,[70] G. Castignani,[3] S. Cavuoti,[64,71] A. Cimatti,[72] C. Colodro-Conde,[15] G. Congedo,[43] L. Conversi,[50,73] F. Courbin,[74,75,76] H. M. Courtois,[77] M. Cropper,[78] J.-G. Cuby,[2,79] A. Da Silva,[80,81] H. Degaudenzi,[82] G. De Lucia,[54] A. M. Di Giorgio,[49] C. Dolding,[78] F. Dubath,[82] C. A. J. Duncan,[40] X. Dupac,[50] A. Ealet,[18] M. Farina,[49] F. Faustini,[23,60] N. Fourmanoit,[33] M. Frailis,[54] S. Galeotta,[54] K. George,[28] C. Giocoli,[3,58] B. R. Granett,[52] A. Grazian,[31] F. Grupp,[27,28] L. Guzzo,[52,83,84] S. V. H. Haugan,[85] J. Hoar,[50] H. Hoekstra,[24] W. Holmes,[4] I. Hook,[86] F. Hormuth,[87] A. Hornstrup,[88,89] P. Hudelot,[38] M. Jhabvala,[90] B. Joachimi,[91] E. Keihänen,[92] S. Kermiche,[33] B. Kubik,[18] K. Kuijken,[24] M. Kunz,[93] H. Kurki-Suonio,[94,95] P. B. Lilje,[85] V. Lindholm,[94,95] I. Lloro,[96] G. Mainetti,[97] D. Maino,[30,83,84] E. Maiorano,[3] O. Mansutti,[54] O. Marggraf,[98] K. Markovic,[4] M. Martinelli,[23,99] N. Martinet,[2] F. Marulli,[3,29,58] R. Massey,[100] S. Mei,[101,102] Y. Mellier,[38,103] M. Meneghetti,[3,58] E. Merlin,[23] G. Meylan,[74] A. Mora,[104] L. Moscardini,[3,29,58] C. Neissner,[69,105] S.-M. Niemi,[106] J. W. Nightingale,[107] C. Padilla,[105] S. Paltani,[82] F. Pasian,[54] K. Pedersen,[108] W. J. Percival,[109,110,111] V. Pettorino,[106] G. Polenta,[60] M. Poncet,[59] L. A. Popa,[112] L. Pozzetti,[3] F. Raison,[27] R. Rebolo,[15,16,113] A. Renzi,[32,34] J. Rhodes,[4] G. Riccio,[64] E. Romelli,[54] M. Roncarelli,[3] E. Rossetti,[57] R. Saglia,[27,28] Z. Sakr,[114,115,116] D. Sapone,[117] B. Sartoris,[28,54] J. A. Schewtschenko,[43] M. Schirmer,[1] P. Schneider,[98] T. Schrabback,[118] A. Secroun,[33] E. Sefusatti,[53,54,55] G. Seidel,[1] M. Seiffert,[4] S. Serrano,[48,119,120] G. Sirri,[58] L. Stanco,[32] J. Steinwagner,[27] P. Tallada-Crespí,[68,69] A. N. Taylor,[43] H. I. Teplitz,[121] I. Tereno,[80,122] S. Toft,[89,123] R. Toledo-Moreo,[124] F. Torradeflot,[68,69] I. Tutusaus,[115] L. Valenziano,[3,125] J. Valiviita,[94,95] T. Vassallo,[28,54] G. Verdoes Kleijn,[126] A. Veropalumbo,[52,61,62] Y. Wang,[121] J. Weller,[27,28] F. M. Zerbi,[52] E. Zucca,[3] M. Bolzonella,[3] C. Burigana,[125,127] R. Cabanac,[115] L. Gabarra,[128] V. Scottez,[103,129] M. Viel[53,54,55,56,130] and D. Scott[131]

Affiliations are listed at the end of the paper

★ E-mail: banados@mpia.de

† VLB would like to dedicate this paper to the memory of Bianca Garalli, who passed away on 2024 September 20, for her invaluable contribution to the *Euclid* spectroscopic pipeline.

ABSTRACT

We demonstrate the potential of *Euclid* 's slitless spectroscopy to discover high-redshift ($z > 5$) quasars and their main photometric contaminant, ultracool dwarfs. Sensitive infrared spectroscopy from space is able to efficiently identify both populations, as demonstrated by *Euclid* Near-Infrared Spectrometer and Photometer Red Grism (NISP RG_E) spectra of the newly discovered $z = 5.404$ quasar EUCL J181530.01+652054.0, as well as several ultracool dwarfs in the *Euclid* Deep Field North and the *Euclid* Early Release Observation field Abell 2764. The ultracool dwarfs were identified by cross-correlating their spectra with templates. The quasar was identified by its strong and broad C III] and Mg II emission lines in the NISP RG_E 1206–1892 nm spectrum, and confirmed through optical spectroscopy from the Large Binocular Telescope. The NISP Blue Grism (NISP BG_E) 926–1366 nm spectrum confirms C IV and C III] emission. NISP RG_E can find bright quasars at $z \approx 5.5$ and $z \gtrsim 7$, redshift ranges that are challenging for photometric selection due to contamination from ultracool dwarfs. EUCL J181530.01+652054.0 is a high-excitation, broad absorption line quasar detected at 144 MHz by the LOw-Frequency Array ($L_{144} = 4.0 \times 10^{25}$ W Hz^{-1}). The quasar has a bolometric luminosity of 3×10^{12} L$_\odot$ and is powered by a 3.4×10^9 M$_\odot$ black hole. The discovery of this bright quasar is noteworthy as fewer than one such object was expected in the ≈ 20 deg^2 surveyed. This finding highlights the potential and effectiveness of NISP spectroscopy in identifying rare, luminous high-redshift quasars, previewing the census of these sources that *Euclid*'s slitless spectroscopy will deliver over about 14 000 deg^2 of the sky.

Key words: stars: brown dwarfs – stars: individual: EUCL J174429.80 + 672728.1, EUCL J002516.31-491618.5 – quasars: individual: EUCL J181530.01 + 652054.0.

1 INTRODUCTION

Quasars are accreting supermassive black holes in the centres of massive galaxies that can be studied in detail at large cosmological distances, even within the first Gyr after the big bang. These distant quasars provide important constraints on the formation and growth of supermassive black holes, massive galaxies, the build-up of large-scale structure, and the Universe's last major phase transition, the epoch of reionization (see Fan, Bañados & Simcoe 2023, for a recent review).

Quasars at $z \gtrsim 5$ have traditionally been identified from photometric colour selections (e.g. Jiang et al. 2016; Matsuoka et al. 2019; Belladitta et al. 2025) assisted by machine-learning and probabilistic approaches (e.g. Mortlock et al. 2012; Wenzl et al. 2021; Byrne et al. 2024). Candidates are then confirmed through spectroscopic observations (e.g. Yang et al. 2024). The main challenges to identifying the most distant quasars are (i) the rapid decline of their number density at $z > 5$ (e.g. Matsuoka et al. 2023; Schindler et al. 2023); and (ii) the similar colours of the more abundant late M and L and T brown dwarf populations. Selection effects produce a lack of quasars at $z \approx 5.5$ and between $z = 7.1$ (Mortlock et al. 2011) and $z = 7.5$ (Bañados et al. 2018; Yang et al. 2020; Wang et al. 2021). The first gap is due to the colours of $z \approx 5.5$ quasars being almost indistinguishable from some M and L dwarfs, the most abundant stars in our Galaxy (see e.g. fig. 1 in Bañados et al. 2016 and Matsuoka et al. 2016). Most of the $z \approx 5.5$ quasars known have been discovered through dedicated campaigns to fill this gap (e.g. Yang et al. 2019). The second gap centred at $z \approx 7.3$ is due to the photometric contamination of L and T dwarfs (see e.g. Hewett et al. 2006; Lodieu et al. 2007; Mortlock et al. 2009; Burningham et al. 2013 and fig. 2 in Fan et al. 2023). Currently, there are more than 11 000 spectroscopically confirmed M6–M9, ~ 2200 L, and ~ 800 T ultracool dwarfs (Smart et al. 2019; Best et al. 2024).

The next breakthrough for reionization-era quasar discoveries is expected to come from the *Euclid* mission (Euclid Collaboration 2025d). The Euclid Wide Survey (EWS; Euclid Collaboration 2022a) will cover about 14 000 deg^2 of extragalactic sky in the optical (I_E filter; Euclid Collaboration 2025c) and near-infrared (Y_E, J_E, and

H_E filters; Euclid Collaboration 2022b, 2025b). The expected quasar yields from *Euclid* photometric selection are discussed for $z < 7$ in Euclid Collaboration (2025e) and for $z > 7$ by Euclid Collaboration (2019). Fig. 2 shows that photometric contamination of brown dwarfs is also expected to be one of the main challenges for $z > 5$ quasar identification using only *Euclid* photometry.

In addition to photometry, the Near-Infrared Spectrometer and Photometer (NISP) on *Euclid* also provides grism slitless spectroscopy with a resolving power greater than 480 (for a 0.″5 diameter object) over the range 1206–1892 nm (referred to as the red grism; RG_E; Euclid Collaboration 2025b). The RG_E data are available throughout the entire EWS, while NISP also offers blue grism spectroscopy (BG_E) with a resolving power greater than 400 (for a 0.″5 diameter object) over the range 926–1366 nm, exclusively in the Euclid Deep Survey (EDS), covering approximately 60 deg^2 (Euclid Collaboration 2025b, 2025d). Here, we discuss and demonstrate the potential for discovering quasars (and their contaminants) directly from NISP spectroscopy. Given the low number density of bright quasars at $z > 5$, with only a few expected per 100 deg^2 (Matsuoka et al. 2023; Schindler et al. 2023), we primarily focus on the capabilities of the NISP RG_E, which spans the largest area where significant discoveries are anticipated. Fig. 1 shows the strongest quasar emission lines that fall within the NISP grism wavelength range as a function of redshift. When more than one strong emission line is observed, the quasar nature and redshift can, in principle, be obtained directly from the NISP spectrum.

This paper is structured as follows. We describe the *Euclid* data used for this work in Section 2. In Section 3, we briefly discuss the discovery potential for ultracool dwarfs. In Section 4, we introduce two $z \approx 5.5$ quasar candidates identified with NISP RG_E. We discuss the properties of a newly discovered $z = 5.4$ quasar in Section 5. Finally, in Section 6 we provide a summary and highlight additional science cases enabled by NISP slitless spectra. Appendix A lists the ultracool dwarf templates used in this work. Appendix B provides an example of NISP RG_E two-dimensional spectrograms. In Appendix C, we show NISP BG_E spectra of the $z \approx 5.5$ quasar candidates. We adopt a standard, flat cosmological model with $H_0 = 70$ km s^{-1} Mpc^{-1}
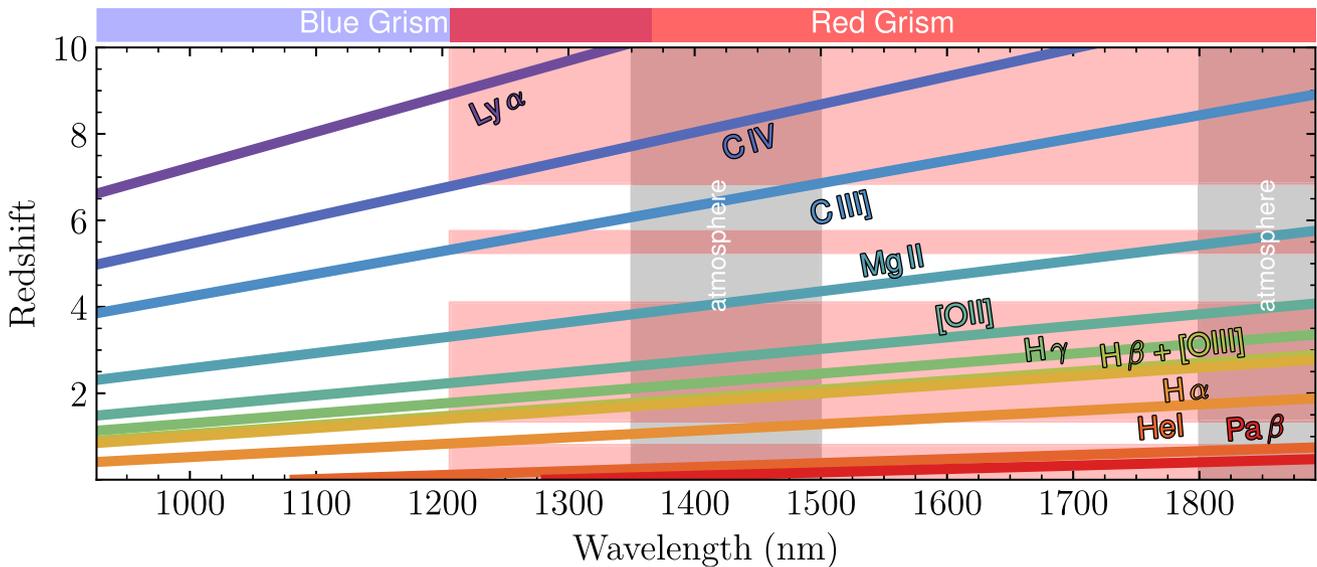
Figure 1. Quasar strong emission lines as a function of redshift within the NISP BG_E and RG_E bandpasses (Euclid Collaboration 2025b), as indicated at the top of the figure. NISP BG_E data will only be available in the EDS, while NISP RG_E data will be present in the EWS. The vertical grey-shaded regions correspond to wavelengths of strong telluric absorption, where ground-based telescopes are not sensitive. The horizontal red-shaded regions represent the redshift ranges with at least two strong emission lines expected in the NISP RG_E spectral bandpass, thereby providing the most reliable redshifts for 'blind' discoveries over the entire EWS.

and $\Omega_m = 0.30$. All *Euclid* magnitudes reported are from aperture photometry in the AB system unless otherwise stated. All postage stamps are oriented north up and east to the left.

2 DATA

In this paper, we use NISP RG_E data from the phase verification campaign in the Euclid Deep Field North (EDF-N; 20 deg^2 centred on RA = $17^h 58^m 55\overset{s}{.}9$ and Dec = $+66°; 01' 04\overset{''}{.}7$) and from the Early Release Observations (ERO; Euclid Early Release Observations 2024) of the lensing cluster Abell 2764, centred on RA = $00^h 22^m 50\overset{s}{.}1$ and Dec = $-49°; 15' 59\overset{''}{.}8$ (Atek et al. 2025).

The EDF-N NISP RG_E grism data were the first validated and made available to the Euclid Consortium. Near the completion of this work, the EDF-N NISP BG_E grism data were made available to the Euclid Consortium for validation. In Appendix C, we showcase some of the first NISP BG_E spectra, and we note that these spectra are not available in the first *Euclid* Quick Data Release (Q1; Euclid Collaboration: Aussel et al. 2025). The data used here are from one Reference Observing Sequence (ROS), equivalent to the depth expected for the EWS. The NISP grism data have been fully processed with the standard *Euclid* pipeline (see Section 7.5 in Euclid Collaboration: Mellier et al. 2025). We use the merged catalogue from the phase verification campaign (mer-pv) for coordinates, photometry, and OBJECT-ID (for details, see section 7.4 in Euclid Collaboration 2025d). The EDF-N also has dedicated deep radio 144 MHz observations (with central RMS noise of $32\,\mu$Jy beam^{-1}) from the LOw-Frequency Array (LOFAR; Bondi et al. 2024).

The grism data in the Abell 2764 field are from three ROS. However, the ERO data have not been processed through the standard *Euclid* pipeline. Indeed, only imaging data products have been published so far, reduced with a custom-made pipeline (Cuillandre et al. 2025). All magnitudes reported in this field are from the catalogue presented in Weaver et al. (2025). To extract spectra,

we performed the following steps. We mosaiced the 16 individual detectors, both for the direct and for the dispersed images, into single images using the world coordinate system from the H_E-band exposures. We derived ad-hoc trace equations for all four grism settings using bright stars, mapping the (x_g, y_g) positions of the start of the spectra and the spectral slope as a function of the (x_i, y_i) positions of the objects in the direct image. Two-dimensional cut-outs were extracted for each object. Spectra with the same grism-angle combinations from different ROS were rectified, combined together and background-subtracted. One-dimensional spectra were extracted using a box-car extraction aperture of seven pixels. The wavelength was calibrated against a handful of emission line objects with known redshifts in the Abell 2764 field. Even though the variation of the wavelength solution across the field has not been mapped in detail, the above model proves sufficiently accurate for the current investigation (see Section 3.1).

3 IDENTIFICATION OF ULTRACOOL DWARFS WITH *Euclid* NISP GRISM

Our primary goal is to use NISP RG_E data to identify quasars at $z \approx 5.5$ and $z \gtrsim 7$ (Fig. 1). However, current estimates of the quasar luminosity function (Matsuoka et al. 2023; Schindler et al. 2023) suggest that there are fewer than 0.3 and 0.04 bright quasars (with $M_{1450} < -25.5$) in about 20 deg^2 at $z \approx 5.5$ and $z \gtrsim 7$, respectively. Consequently, the initial goal of this study was to examine the NISP spectra of typical contaminants for high-redshift quasars, particularly the far more numerous ultracool dwarfs.

Thus, in addition to the templates used to determine redshifts through template fitting described in Section 7.5.2 of Euclid Collaboration (2025d), we include M-, L-, and T-dwarf templates from the SpeX Prism Spectral Libraries (Burgasser 2014), which we list in Appendix A. The main limitation of the present work is the restricted number of templates used for classification. However, resampling the
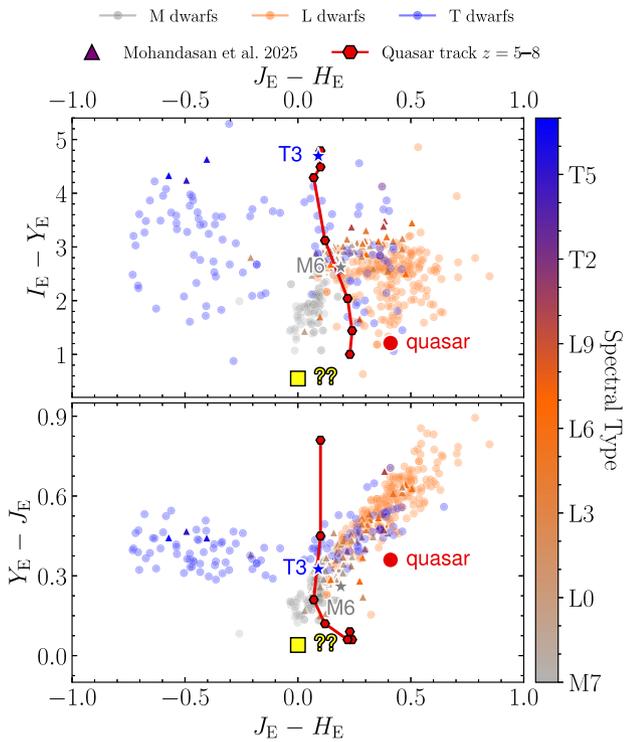
Figure 2. Top: (Bottom:) $I_E - Y_E$ ($Y_E - J_E$) versus $J_E - H_E$ diagram showing the synthetic colours of the M-, L-, and T-dwarfs from the SpeX Prism Library (small circles), as measured by Weaver et al. (2025). The triangles represent ultracool dwarfs discussed in Mohandasan et al. (2025), with spectral types indicated by the colour bar. The solid line represents the colour track of the $z = 6$ quasar composite spectrum of Bañados et al. (2016) combined at rest-frame 1300 Å with the average spectrum of Vanden Berk et al. (2001). The hexagonal markers are plotted in steps of $\Delta z = 0.5$, starting at $z = 5$ at the bottom and finishing at $z = 8$ at the top. The larger, labelled symbols represent the colours of the individual sources discussed in this paper: the T3 dwarf EUCL J002516.31−491618.5 (blue star), the M6 dwarf EUCL J174429.80+672728.1 (grey star), the $z = 5.4$ quasar EUCL J181530.01+652054.0 (red circle), and the unidentified source EUCL J180409.14+641335.3 (yellow square). These colour-colour diagrams are for context, and we emphasize that *Euclid* photometry was not used to identify these sources (except the T3 dwarf; see Section 3.1).

spectra, we find that our classification is robust within ±1 spectral type. Indeed, this experiment recovered known ultracool dwarfs in the field and enabled the discovery and confirmation of 33 new ones ranging from M7 to T1, which are presented in detail in Mohandasan et al. (2025). In this paper, we will present examples of two new ultracool dwarfs, which are not in the sample of Mohandasan et al. (2025).

3.1 A new T3 dwarf in the ERO field Abell 2764

We selected EUCL J002516.31−491618.5 as a potential high-redshift quasar candidate based on a large $I_E - Y_E > 4$ colour and flat NISP colours (see Fig. 2 and the top panel of Fig. 3). We used the photometry reported in the catalogue of Weaver et al. (2025) (CATALOG ID = 373511).

The source EUCL J002516.31−491618.5 is the brightest and one of the most promising $z > 6$ quasar candidates in the Abell 2764 field. However, the chances of identifying a $Y_E < 19$ quasar at $z > 6$ in just 0.75 deg² are negligible (Matsuoka et al. 2023; Schindler et al. 2023).

If this were indeed a quasar, it would be among the most luminous sources ever reported in the early Universe (Wu et al. 2015; Fan et al. 2019). To confirm or refute this potentially remarkable serendipitous discovery, we developed our own pipeline to extract the *Euclid* NISP spectrum of these ERO data (see Section 2). Fig. 3 shows the extracted spectrum, which clearly classifies the source as a brown dwarf. We note that this object was photometrically identified as a T3 candidate by dal Ponte et al. (2023). Resampling the spectrum reveals that the best match template varies between T3 and T4, although visually, neither template is a perfect match. The template of a T3 binary, 2MASSJ12095613−1004008 (Burgasser et al. 2004; Dupuy & Liu 2012), appears to be a visually better match (plotted in Fig. 3), suggesting that it could also be a T binary.

3.2 A new M6 dwarf in the EDF-N

Object EUCL J174429.80+672728.1 (OBJECT-ID = 2661241859674578148) was first selected as a $z \approx 5.6$ quasar candidate from the Pan-STARRS1 survey (Bañados et al. 2023), but rejected as a quasar after a follow-up observation with the Multi-Object Double Spectrograph (MODS; Pogge et al. 2010) at the Large Binocular Telescope (LBT). The LBT/MODS observations were carried out in dual mode on 2017 April 21 and June 5. The red grating G670L and a 1.2 arcsec slit were used for a total exposure time of 1 h. We present the LBT spectrum for the first time here (the bottom panel of Fig. 4).

The MODS spectrum was reduced with the open-source PYTHON-based Spectroscopic Data Reduction Pipeline PYPEIT[1] (version 1.14.1; Prochaska et al. 2020). With that pipeline, we perform image processing, including gain correction, bias subtraction, and flat fielding. The extracted spectrum was flux-calibrated with a sensitivity function derived from the observation of a spectroscopic standard star. The spectra were then co-added and absolute flux calibrated to match the I_E magnitude.

Since this quasar candidate is located in the EDF-N, we analysed the *Euclid* grism spectrum independently of the existing LBT spectrum. The best-fitting template was an M6 dwarf, shown in the middle panel of Fig. 4. The M6 dwarf template is relatively featureless in the 1200–1900 nm regime. Notably, the same template reproduces the optical features seen in the LBT spectrum (the bottom panel of Fig. 4). By resampling the *Euclid* spectrum, we find that approximately 95 per cent of the cases classify this source as an M6, 4 per cent as an M7, and 1 per cent as an M8 type. *Euclid* cut-outs and photometry are shown in the top panel of Fig. 4.

4 IDENTIFICATION AND FOLLOW-UP OBSERVATIONS OF z > 5 Euclid QUASAR CANDIDATES

We added the quasar composite spectrum of Vanden Berk et al. (2001) as part of the redshift template fitting of the *Euclid* pipeline in order to be able to identify $z > 5$ quasars. In the EDF-N field, there were only two sources for which the quasar template was the best match and at an implied redshift where two strong emission lines are expected in the NISP RG$_E$ spectra (Fig. 1). This was a selection based purely on the NISP RG$_E$ spectra matched to templates; no photometry or additional information was used. For completeness, we show the NISP BG$_E$ spectra of these sources in Appendix C.
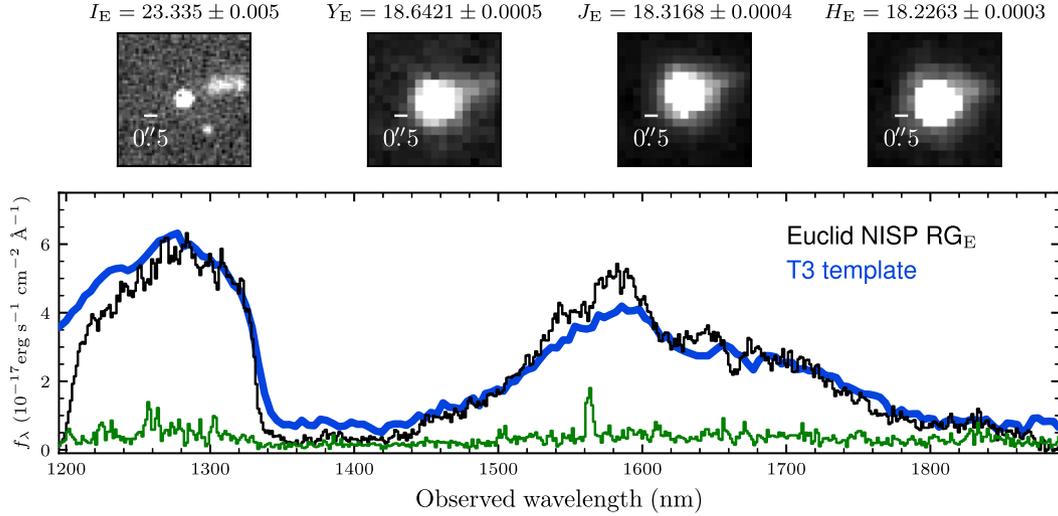
---

[1] https://github.com/pypeit/PypeIt

Figure 3. *Top:* Postage stamps of the T3 dwarf EUCL J002516.31−491618.5. The *Euclid* I_E, Y_E, J_E, and H_E images are $5\,arcsec$ on a side. *Bottom:* NISP RG$_E$ grism spectrum (black line and the uncertainties in green). The blue line shows a template of a T3 binary: 2MASS J12095613−1004008 (Burgasser et al. 2004; Dupuy & Liu 2012).
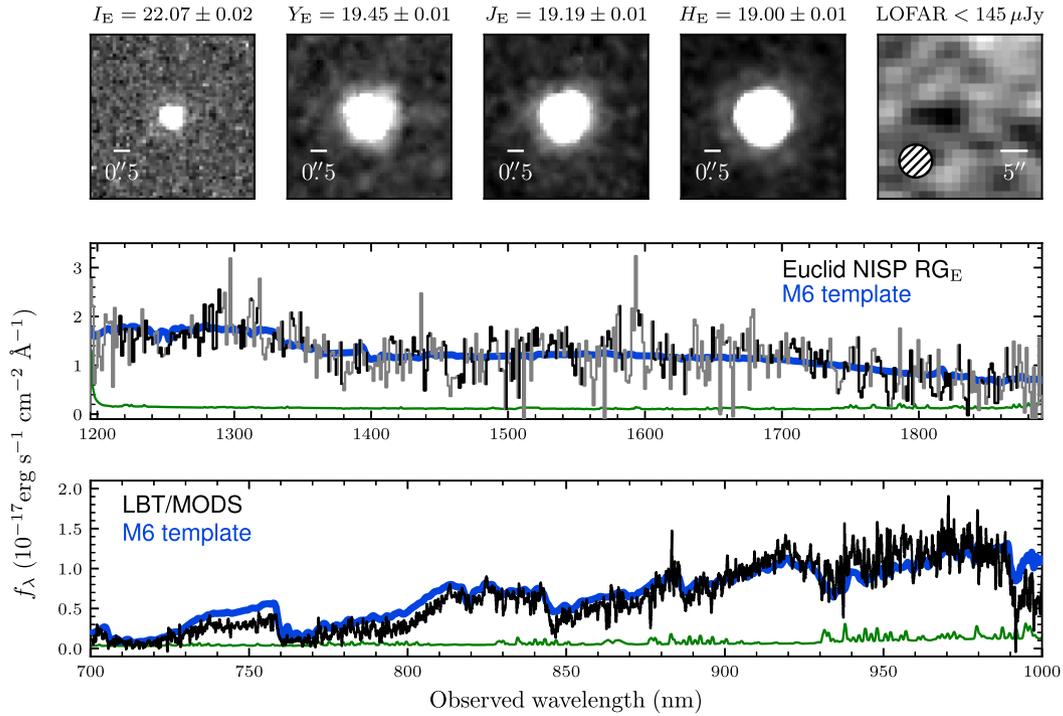

Figure 4. *Top:* Postage stamps of the M6 dwarf EUCL J174429.80+672728.1. The *Euclid* I_E, Y_E, J_E, and H_E images are 5″ on a side, while the LOFAR image is 30 arcsec on a side. The LOFAR beam is shown in the lower left of its panel and the reported flux density corresponds to a 3σ upper limit. *Middle:* NISP RG$_E$ grism spectrum (black line; masked pixels are in grey, and the uncertainties in green). The blue line shows the best template fit, identifying this as an M6 dwarf. *Bottom:* LBT/MODS optical spectrum (black line and uncertainties in green), confirming the *Euclid* classification. The spectral features are clearly well-matched to the observed optical spectrum. The template corresponds to LHS 36 (also known as Wolf 359), originally published in Burgasser et al. (2008).

4.1 EUCL J181530.01+652054.0

The quasar template proved to be the best match to the source EUCL J181530.01+652054.0 (hereafter EUCL QSO J1815+6520; `OBJECT-ID = 2738750478653483354`), implying a quasar at $z =$

5.40. The *Euclid* spectra, photometry, and cut-out images of EUCL QSO J1815+6520 are displayed in the top panel of Fig. 5. We visually inspected the *Euclid* spectrum and found that the C III] and Mg II lines were robustly detected and could be well-fitted by single

Figure 5. *Top:* Postage stamps of the $z = 5.4$ quasar EUCL J181530.01+652054.0. The *Euclid* I_E, Y_E, J_E, and H_E images are $5''$ on a side while the LOFAR image is $30''$ on a side. The LOFAR beam is shown on the lower left of its panel. *Middle:* NISP grism RG_E spectrum (black line; masked pixels are in grey, and the uncertainties in green). The blue line shows the best-fitting power-law emission plus C III] and Mg II broad emission lines, identifying this as a quasar at $z_{Mg II} = 5.404 \pm 0.007$. *Bottom:* LBT/MODS optical spectrum (black line and uncertainties in green), confirming the quasar nature of EUCL J181530.01+652054.0. The vertical dashed lines correspond to the expected position of the labelled emission lines based on the Mg II redshift. The dashed rectangles indicate the Si IV and C IV BAL regions shown in Fig. 7.

Gaussians (Fig. 5), with a Mg II-redshift of $z_{Mg II} = 5.404 \pm 0.007$ (the age of the Universe was 1.04 Gyr at this redshift).

We observed EUCL QSO J1815+6520 with LBT/MODS on 2024 June 17. The observations were carried out in dual mode with the red grating G670L, a slit of $1''$ width, and a total exposure time of 15 min. The spectrum was reduced as described in Section 3.2 and is shown in the bottom panel of Fig. 5, confirming the quasar nature of EUCL QSO J1815+6520. The spectrum reveals a C IV line with an equivalent width of (13 ± 0.4) Å and blueshifted by (2070 ± 330) km s^{-1} with respect to the Mg II line, consistent with quasars displaying strong broad-line region outflows (e.g. Vietri et al. 2018; Rankine et al. 2020; Gillette & Hamann 2024). We measured the rest-frame absolute magnitude at 1450 Å directly from the LBT spectrum, resulting in $M_{1450} = -25.52 \pm 0.01$.

4.2 EUCL J180409.14+641335.3

The template fitting of EUCL J180409.14+641335.3 (OBJECT-ID = 2710381121642264965), implied a quasar at $z = 5.37$. The *Euclid* spectrum, cut-outs, and photometry are shown in the top panel of Fig. 6.

The visual inspection of the spectrum is not as convincing as that of EUCL QSO J1815+6520. The feature that is expected to be Mg II at $z = 5.37$ is broader than the quasar template and the existence of C III] is unclear (Fig. 6).

To come full circle on testing this quasar-discovery strategy, we obtained follow-up optical spectroscopy with the Double Spectrograph (DBSP; Oke & Gunn 1982) on the 5-m Hale telescope at Palomar Observatory on 2024 July 10. We obtained three exposures of 1200 s

each using the 1.5 arcsec slit. The data were reduced analogously to the LBT spectrum described in Section 3.2, but with the PYPEIT version 1.16.0. The Palomar/DBSP spectrum (the bottom panel of Fig. 6) does not show the sharp break expected at $0.77\,\mu$m for a $z = 5.4$ quasar (compare with the LBT spectrum in Fig. 5). Indeed, the Palomar spectrum does not reveal any strong emission lines, and is relatively featureless. This spectrum is not well reproduced by any of the current templates used in the *Euclid* pipeline, and finding the exact spectral classification is beyond the scope of this work.

5 PHYSICAL PROPERTIES OF THE $z = 5.4$ *Euclid* QUASAR

5.1 Black hole mass

The *Euclid* spectrum of EUCL QSO J1815+6520 covers the broad Mg II emission line (the middle panel of Fig. 5), which is one of the most reliable tracers to derive single-epoch, black hole mass measurements (e.g. Fan et al. 2023). It is not possible to study Mg II from the ground at $z \approx 5.4$ due to the low atmospheric transparency at around 1800 nm (Fig. 1).

We use the relationship presented in Vestergaard & Osmer (2009) to estimate the black hole mass from the full-width at half maximum of the Mg II line [$FWHM_{Mg II} = (5138 \pm 616)$ km s^{-1}] and the luminosity at 3000 Å [$L_{3000} = (5.7 \pm 0.2) \times 10^{12} L_\odot$], yielding $M_{BH} = (3.0 \pm 0.7) \times 10^9 M_\odot$. Adopting a widely used bolometric correction ($L_{Bol} = 5.15 L_{3000}$; see e.g. Mazzucchelli et al. 2023), we find an Eddington ratio of $L_{Bol} / L_{Edd} = 0.3 \pm 0.1$. These properties
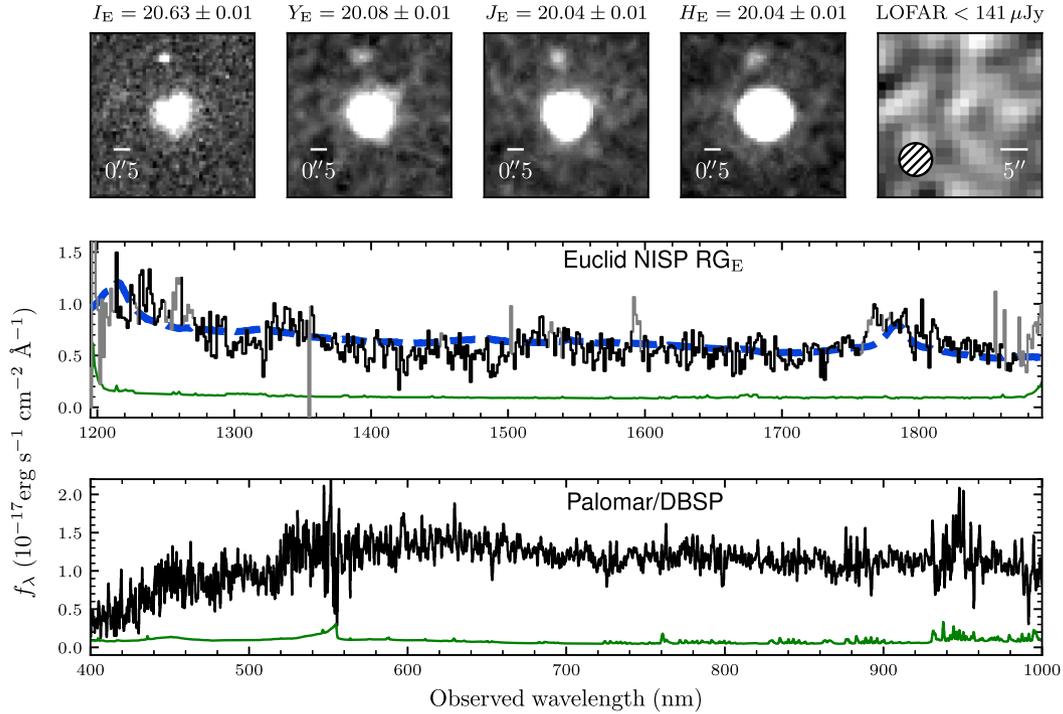
Figure 6. *Top:* Postage stamps of the quasar candidate EUCL J180409.14+641335.3. The *Euclid* I_E, Y_E, J_E, and H_E images are 5 arcsec on a side while the LOFAR image is 30 arcsec on a side. The LOFAR beam is shown in the lower left of its panel and the reported flux density corresponds to a 3σ upper limit. *Middle:* NISP RG_E grism spectrum (black line; masked pixels are in grey and the uncertainties in green). The dashed blue line shows the best-fitting template corresponding to a quasar (Vanden Berk et al. 2001) redshifted to $z = 5.37$. *Bottom:* Palomar/DBSP optical spectrum (black line and uncertainties in green, revealing a relatively flat spectrum, ruling out EUCL J180409.14+641335.3 being a $z \sim 5.4$ quasar.

are consistent with the bulk of the quasars studied at $z \gtrsim 5$ (e.g. Shen et al. 2019; Lai et al. 2024).

5.2 BAL properties

The LBT spectrum of EUCL QSO J1815+6520 (the bottom panel of Fig. 5) not only validates the *Euclid* discovery but also reveals strong absorption features blueward of N V, Si IV, and C IV, classifying this source as a high-excitation, broad absorption line (BAL) quasar. The presence of BALs in quasar spectra indicates strong outflows, launched from accretion discs, that can have velocities of up to 20 per cent of the speed of light (c; e.g. Rodríguez Hidalgo et al. 2020). The exact fraction of BAL quasars is still debated, but it ranges from 10 to 50 per cent (Dai, Shankar & Sivakoff 2008; Allen et al. 2011; Bischetti et al. 2022).

The N V BAL in EUCL QSO J1815+6520 coincides with the wavelengths absorbed by foreground neutral hydrogen in the intergalactic medium (Fig. 5). Thus, we cannot determine its velocity structure confidently, and instead we focus on the Si IV and C IV BALs. We use the task `continuumfit` from the `linetools` PYTHON package[2] to interactively fit the quasar continuum and then normalize its flux. Fig. 7 shows the normalized spectra around the BAL regions highlighted in Fig. 5. The detached and terminal velocities quantify the minimum and maximum outflow velocities of the gas traced by the BAL (Hall et al. 2002). To be conservative, we measured the BAL minimum detached and terminal velocities

from the 90 per cent level of the normalized spectrum. We obtained the same range of velocity for both BALs, 0.015–0.041 c, indicating that they originate from the same kinematic region (see Fig. 7). This quasar has a C IV balnicity index (BI; Weymann et al. 1991) of $BI = 3766^{+1128}_{-1809}$ km s^{-1}, indicating a powerful outflow (e.g. Bischetti et al. 2022).

5.3 Radio properties

The quasar EUCL QSO J1815+6520 is well-detected in the LOFAR 144 MHz data shown in the top panel of Fig. 5. The source is outside of the central circular 10 deg^2 region used to create the LOFAR-EDF-N catalogue (Bondi et al. 2024). Thus, we measured the flux density directly from the beam-corrected image.[3] The source is unresolved, and we measure a peak flux density of $(481 \pm 46)\,\mu$Jy. We note that the radio data were not used for the selection of the quasar, and that late M-dwarfs can also show comparable radio emission (Gloudemans et al. 2023).

Radio-loudness in quasars is an observational parameter used to quantify the power of synchrotron radiation with respect to emission in the UV/optical regime coming from the accretion disc. The radio-loudness is usually defined as the ratio of the flux densities at rest-frame 5 GHz and 2500 Å or 4400 Å. Here, we use the former definition, R_{2500}, since rest-frame 2500 Å is covered by the *Euclid* spectrum, while for 4400 Å we would need to extrapolate. Since we only have a radio detection at 144 MHz, we

---

[2] https://github.com/linetools

[3] https://lofar-surveys.org/deepfields_public_edfn.html

Figure 7. Normalized LBT/MODS spectrum of EUCL QSO J1815+6520 zoomed-in on the BAL regions (see Fig. 5 and Section 5.2). The solid and dashed horizontal lines correspond to 100 per cent and 90 per cent of the normalized spectrum, respectively. The vertical dotted lines and the blue-shaded region show that the Si IV (top) and C IV (bottom) outflows have velocities 0.015–0.041 c.

extrapolate to rest-frame 5 GHz assuming the median spectral index $\alpha = -0.29$ (in the convention $f_\nu \propto \nu^\alpha$), following Gloudemans et al. (2021). We obtain a radio-loudness of $R_{2500} = 9 \pm 1$, which places EUCL QSO J1815+6520 at the boundary between sources classified as radio-quiet or radio-loud (Kellermann et al. 1989; Jiang et al. 2007; but see also Calistro Rivera et al. 2024). The uncertainty reported does not consider the uncertainty on the radio extrapolation. The rest-frame 144 MHz specific radio luminosity is $L_{144} = (4.0 \pm 0.4) \times 10^{25}$ W Hz^{-1}, similar to the bulk of $z > 5$ quasars detected with LOFAR (see e.g. Fig. 4 in Gloudemans et al. 2021). If we assume a radio spectral index $\alpha = -0.7$ instead, the radio-loudness and 144 MHz specific radio luminosity would be $R_{2500} = 4.6 \pm 0.5$ and $L_{144} = (8.6 \pm 0.8) \times 10^{25}$ W Hz^{-1}, respectively.

We can conclude that EUCL QSO J1815+6520 has an intermediate radio-loudness of $R_{2500} = 4$–10 (depending on the radio spectral index; see above). However, the radio emission might not only come from synchrotron emission from the relativistic jet, because the quasar also shows evidence of outflows through high excitation BAL features (Section 5.2): As shown by Petley et al. (2022), BAL quasars are more likely to be detected at 144 MHz than their non-BAL counterparts, which suggests that shocks may cause part of the radio emission due to the BAL outflows interacting with the interstellar medium in their host galaxies. Additional radio detections at other frequencies are required to interpret the radio properties of this source.

6 SUMMARY AND OUTLOOK

We have demonstrated that *Euclid* slitless infrared spectroscopy is a powerful tool to identify quasars and to eliminate confusion with ultracool dwarfs by cross-correlating NISP RG$_E$ spectra with templates. The NISP RG$_E$ spectral coverage is particularly well-matched to strong spectral features in L and T dwarfs (Fig. 3, and Mohandasan et al. 2025), but it can also help with the classifications for objects with less prominent spectral features in the 1206–1892 nm spectral range, such as late M dwarfs (Fig. 4). Without the spectroscopic information, the ultracool dwarfs discussed here could mistakenly have been selected as high-redshift quasar candidates. Similar but more distant (thus fainter) brown dwarfs could incorrectly have been selected as high-redshift galaxies (e.g. Roberts-Borsani et al. 2025). Atek et al. (2025) argue that requiring $I_E - Y_E > 3$ reduces contamination by brown dwarfs. However, as shown in Fig. 2, late L- and T-dwarfs with such a significant colour break do exist and, therefore, brown dwarfs can still be a substantial contaminant to the $z > 6$ galaxy candidates presented in Weaver et al. (2025).

In this paper, we focus on the highest redshift quasars to explore how efficiently *Euclid* can help to fill the quasar redshift gaps at $z \approx 5.5$ and $z \gtrsim 7$, where NISP RG$_E$ spectra allow us to identify two emission lines (Fig. 1). In the future, we will combine the grism data with photometric information (see Fig. 2). In that case, having even only one (or zero) strong emission line in the NISP RG$_E$ spectra will help constrain the source redshift. Additionally, in the EDS, the expanded wavelength coverage provided by the NISP BG$_E$ spectra can be effectively utilized for the reliable identification of sources (see Fig. 1 and Appendix C).

We have identified two sources in the EDF-N for which the best-fitting template is the quasar composite spectrum from Vanden Berk et al. (2001) at a redshift where two emission lines were expected. This blind experiment already showcases the potential of *Euclid* for new quasar discoveries. The most promising source, with clear detections of the C III] and Mg II lines, was confirmed as a quasar at the expected $z = 5.4$ redshift with an optical follow-up spectrum (Fig. 5). However, for the second candidate, no obvious emission lines were detected in the *Euclid* spectrum or its follow-up, ground-based optical spectrum. The lack of a strong Lyman break rules out a source at $z \gtrsim 3.5$.

The confirmation of EUCL QSO J1815+6520 at $z = 5.4$ is noteworthy, especially considering that we anticipated finding fewer than one quasar of this kind in the surveyed area (Schindler et al. 2023). It is also important to point out that while Data Release 1 of the Dark Energy Spectroscopic Instrument (DESI) covered the EDF-N region and discovered hundreds of new quasars (DESI Collaboration 2025), they excluded follow-up of $z \sim 5.4$–5.6 candidates due to a high expected contamination rate from M-dwarfs (Yang et al. 2023). This emphasizes the potential of NISP RG$_E$ to effectively identify rare sources that may not be easily recognized through photometric methods. Across the entire EWS, this technique could potentially reveal around 400 quasars at $z \approx 5.5$, similar to EUCL QSO J1815+6520, as well as about 30 quasars at $z \gtrsim 7$.

A future improvement to a *Euclid* grism-based selection is to include quasar templates with different spectral properties from those used in this work (e.g. Temple, Hewett & Banerji 2021; Euclid Collaboration 2024). This can result in discovering additional quasars with different dust reddening or weaker/stronger emission lines than those of the average Vanden Berk et al. quasar.

As a final note, *Euclid* grism slitless spectroscopy will allow black hole mass measurements for thousands of (known and new) quasars, for which key emission lines such as C IV, Mg II, H β, and H α, are not visible from the ground (Fig. 1).

DATA AVAILABILITY

The data used in this study can be accessed from the observatories' public archives or the websites of the surveys mentioned in the acknowledgments. The data sets generated and analysed during this study are available from the corresponding author upon reasonable request.

REFERENCES

Allen J. T., Hewett P. C., Maddox N., Richards G. T., Belokurov V., 2011, MNRAS, 410, 860
Atek H., et al., 2025, A&A, 697, A15
Bañados E. et al., 2016, ApJS, 227, 11
Bañados E. et al., 2018, Nature, 553, 473
Bañados E. et al., 2023, ApJS, 265, 29
Belladitta S. et al., 2025, A&A, 699, A335
Best W. M. J., Dupuy T. J., Liu M. C., Sanghi A., Siverd R. J., Zhang Z., 2024, The UltracoolSheet: Photometry, Astrometry, Spectroscopy, and Multiplicity for 4000 + Ultracool Dwarfs and Imaged Exoplanets, https://doi.org/10.5281/zenodo.13993077
Bischetti M. et al., 2022, Nature, 605, 244
Bondi M. et al., 2024, A&A, 683, A179
Burgasser A. J., 2014, in Astronomical Society of India Conference Series. p. 7, preprint (arXiv:1406.4887)
Burgasser A. J., Burrows A., Kirkpatrick J. D., 2006b, ApJ, 639, 1095
Burgasser A. J., Cruz K. L., Cushing M., Gelino C. R., Looper D. L., Faherty J. K., Kirkpatrick J. D., Reid I. N., 2010, ApJ, 710, 1142
Burgasser A. J., Geballe T. R., Leggett S. K., Kirkpatrick J. D., Golimowski D. A., 2006a, ApJ, 637, 1067
Burgasser A. J., Liu M. C., Ireland M. J., Cruz K. L., Dupuy T. J., 2008, ApJ, 681, 579
Burgasser A. J., McElwain M. W., Kirkpatrick J. D., Cruz K. L., Tinney C. G., Reid I. N., 2004, AJ, 127, 2856
Burningham B. et al., 2013, MNRAS, 433, 457
Byrne X., Meyer R. A., Farina E. P., Bañados E., Walter F., Decarli R., Belladitta S., Loiacono F., 2024, MNRAS, 530, 870
Calistro Rivera G. et al., 2024, A&A, 691, A191
Chiu K., Fan X., Leggett S. K., Golimowski D. A., Zheng W., Geballe T. R., Schneider D. P., Brinkmann J., 2006, AJ, 131, 2722
Cuillandre J.-C. et al., 2025, A&A, 697, A6
Dai X., Shankar F., Sivakoff G. R., 2008, ApJ, 672, 108
dal Ponte M. et al., 2023, MNRAS, 522, 1951

DESI Collaboration, 2025, preprint (arXiv:2503.14745)
Dupuy T. J., Liu M. C., 2012, ApJS, 201, 19
Euclid Collaboration, 2019, A&A, 631, A85
Euclid Collaboration, 2022a, A&A, 662, A112
Euclid Collaboration, 2022b, A&A, 662, A92
Euclid Collaboration, 2024, A&A, 685, A108
Euclid Collaboration, 2025a, A&A, submitted (Euclid Q1 SI), preprint (arXiv:2503.15302)
Euclid Collaboration, 2025b, A&A, 697, A3
Euclid Collaboration, 2025c, A&A, 697, A2
Euclid Collaboration, 2025d, A&A, 697, A1
Euclid Collaboration, 2025e, A&A, 693, A250
Euclid Early Release Observations, 2024, https://doi.org/10.57780/esa-qmocze3
Fan X. et al., 2019, ApJ, 870, L11
Fan X., Bañados E., Simcoe R. A., 2023, ARA&A, 61, 373
Gillette J., Hamann F., 2024, MNRAS, 528, 6425
Gloudemans A. J. et al., 2021, A&A, 656, A137
Gloudemans A. J. et al., 2023, A&A, 678, A161
Hall P. B. et al., 2002, ApJS, 141, 267
Hewett P. C., Warren S. J., Leggett S. K., Hodgkin S. T., 2006, MNRAS, 367, 454
Jiang L. et al., 2016, ApJ, 833, 222
Jiang L., Fan X., Ivezić Ž., Richards G. T., Schneider D. P., Strauss M. A., Kelly B. C., 2007, ApJ, 656, 680
Kellermann K. I., Sramek R., Schmidt M., Shaffer D. B., Green R., 1989, AJ, 98, 1195

Kirkpatrick J. D. et al., 2010, ApJS, 190, 100

Kirkpatrick J. D., Barman T. S., Burgasser A. J., McGovern M. R., McLean I. S., Tinney C. G., Lowrance P. J., 2006, ApJ, 639, 1120

Lai S., Onken C. A., Wolf C., Bian F., Fan X., 2024, MNRAS, 527, 3912

Lodieu N. et al., 2007, MNRAS, 379, 1423

Looper D. L. et al., 2008, ApJ, 686, 528

Looper D. L., Kirkpatrick J. D., Burgasser A. J., 2007, AJ, 134, 1162

Matsuoka Y. et al., 2016, ApJ, 828, 26

Matsuoka Y. et al., 2019, ApJ, 872, L2

Matsuoka Y. et al., 2023, ApJ, 949, L42

Mazzucchelli C. et al., 2023, A&A, 676, A71

Mohandasan A., Smart R. L., Reylé C. et al., 2025, A&A, submitted (Euclid Q1 SI), preprint (arXiv:2503.22559)

Mortlock D. J. et al., 2009, A&A, 505, 97

Mortlock D. J. et al., 2011, Nature, 474, 616

Mortlock D. J., Patel M., Warren S. J., Hewett P. C., Venemans B. P., McMahon R. G., Simpson C., 2012, MNRAS, 419, 390

Muench A. A., Lada C. J., Luhman K. L., Muzerolle J., Young E., 2007, AJ, 134, 411

Oke J. B., Gunn J. E., 1982, PASP, 94, 586

Petley J. W. et al., 2022, MNRAS, 515, 5159

Pogge R. W. et al., 2010, Proc SPIE Vol. 7735, Ground-based and Airborne Instrumentation for Astronomy III. SPIE, Belingham, p. 77350A

Prochaska J. et al., 2020, J. Open Source Softw., 5, 2308

Rankine A. L., Hewett P. C., Banerji M., Richards G. T., 2020, MNRAS, 492, 4553

Roberts-Borsani G. et al., 2025, ApJ, 983, 18

Rodríguez Hidalgo P., Khatri A. M., Hall P. B., Haas S., Quintero C., Khatu V., Kowash G., Murray N., 2020, ApJ, 896, 151

Schindler J.-T. et al., 2023, ApJ, 943, 67

Shen Y. et al., 2019, ApJ, 873, 35

Sheppard S. S., Cushing M. C., 2009, AJ, 137, 304

Siegler N., Close L. M., Burgasser A. J., Cruz K. L., Marois C., Macintosh B., Barman T., 2007, AJ, 133, 2320

Smart R. L., Marocco F., Sarro L. M., Barrado D., Beamín J. C., Caballero J. A., Jones H. R. A., 2019, MNRAS, 485, 4423

Temple M. J., Hewett P. C., Banerji M., 2021, MNRAS, 508, 737

van Haarlem M. P. et al., 2013, Astronomy & Astrophysics, 556, A2

Vanden Berk D. E. et al., 2001, AJ, 122, 549

Vestergaard M., Osmer P. S., 2009, ApJ, 699, 800

Vietri G. et al., 2018, A&A, 617, A81

Wang F. et al., 2021, ApJ, 907, L1

Weaver J., Taamoli S., McPartland C. et al., 2025, A&A, 697, A16

Wenzl L. et al., 2021, AJ, 162, 72

Weymann R. J., Morris S. L., Foltz C. B., Hewett P. C., 1991, ApJ, 373, 23

Wu X.-B. et al., 2015, Nature, 518, 512

Yang D.-M. et al., 2024, MNRAS, 528, 2679

Yang J. et al., 2019, ApJ, 871, 199

Yang J. et al., 2020, ApJ, 897, L14

Yang J. et al., 2023, ApJS, 269, 27

APPENDIX A: ULTRACOOL DWARF TEMPLATES

The spectral benchmarks used as templates in this work are listed in Table A1.

Table A1. Spectral benchmarks used as templates in this work.

Spectral Type	Name	Reference
M6	LHS 36	Burgasser et al. (2008)
M7	ITG2	Muench et al. (2007)
M8	KPNO6	Muench et al. (2007)
M9	KPNO12	Muench et al. (2007)
L0	2MASSJ12474944−1117551	Kirkpatrick et al. (2010)
L1	2MASSJ14313097+1436539	Sheppard & Cushing (2009)
L2	2MASSJ01415823−4633574	Kirkpatrick et al. (2006)
L3	SDSSJ213352.72+101841.0	Chiu et al. (2006)
L4	2MASSJ03001631+2130205	Kirkpatrick et al. (2010)
L5	2MASSIJ1526140+204341	Burgasser et al. (2004)
L6	SDSSJ134203.11+134022.2	Chiu et al. (2006)
L7	2MASSJ21481628+4003593	Looper et al. (2008)
L8	2MASSJ10430758+2225236	Siegler et al. (2007)
L9	SDSSJ213154.43−011939.3	Chiu et al. (2006)
T0	Gl337CD	Burgasser et al. (2010)
T1	SDSSJ015141.69+124429.6	Burgasser et al. (2004)
T2	2MASSJ15461461+4932114	Burgasser et al. (2010)
T3	SDSSJ153417.05+161546.1AB	Chiu et al. (2006)
T4	2MASSJ10595219+3041498	Sheppard & Cushing (2009)
T5	2MASSJ18283572−4849046	Burgasser et al. (2004)
T6	2MASSJ16150413+1340079	Looper, Kirkpatrick & Burgasser (2007)
T7	2MASSJ00501994-3322402	Burgasser, Burrows & Kirkpatrick (2006b)
T8	2MASSJ09393548−2448279	Burgasser et al. (2006a)

APPENDIX B: *Euclid* NISP RG$_E$ 2D SPECTROGRAMS

Since this is one of the first publications including NISP RG$_E$ spectra from an ERO program (Euclid Early Release Observations 2024; Atek et al. 2025), we also provide in Fig. B1 the two-dimensional spectrogram for the T dwarf discussed in Section 3.1. Note that these two-dimensional data are not standard products of the *Euclid* pipeline and were processed with a custom pipeline as described in Section 2.

APPENDIX C: *Euclid* NISP BG$_E$ EARLY DATA FOR $z \approx 5.5$ CANDIDATES IN THE EDF-N

As noted in Section 2, the NISP BG$_E$ data from the EDF-N was made available during the final stages of this manuscript. Here, we present the NISP BG$_E$ for the sources discussed in Section 4, showcasing one of the first scientific demonstrations of NISP BG$_E$ data.

Fig. C1 shows all the available spectra for the quasar EUCL QSO J1815+6520. The NISP BG$_E$ bridges the LBT/MODS and NISP RG$_E$ spectra shown in Fig. 5, and the overlapping regions are consistent with each other. From both *Euclid* NISP spectra, three strong emission lines are identified at $z = 5.4$: C IV, C III], and Mg II.

Figure B1. NISP two-dimensional spectrograms of EUCL J002516.31−491618.5. The one-dimensional extraction is shown in Fig. 3. Note that this source is from the Abell 2766 ERO programme and, therefore, has three times more data than the sources from the EWS. Grey regions correspond to missing data.

Figure C1. Spectra of the $z = 5.4$ quasar EUCL QSO J1815+6520. The LBT/MODS (black) and the NISP RG$_E$ (red) spectra were shown in Fig. 5. The NISP BG$_E$ spectrum covers the wavelength range that connects the other two spectra. The uncertainties in the spectra are represented in lighter colours corresponding to each spectrum.

Figure C2. Spectra of the quasar candidate EUCL J180409.14+641335.3 (based solely on NISP RG$_E$ data). The Palomar/DBSP (black) and the NISP RG$_E$ (red) spectra were shown in Fig. 6. The NISP BG$_E$ spectrum covers the wavelength range that connects the other two spectra. The uncertainties in the spectra are represented in lighter colours corresponding to each spectrum. The orange line represents the best template identified by the *Euclid* pipeline, considering both NISP BG$_E$ and RG$_E$ spectra, corresponding to a K-type star.

The C IV BAL is evident in the NISP BG$_E$ spectrum and consistent with the measurements from the LBT/MODS spectrum (Fig. 7).

Fig.C2 shows all the available spectra for the source EUCL J180409.14+641335.3, which was ruled out to be a $z \approx 5.5$ quasar in Section 4.2. The NISP BG$_E$ bridges the Palomar/DBSP and

NISP RG$_E$ spectra shown in Fig. 6, and the overlapping regions are consistent with each other. When analysing both the NISP BG$_E$ and RG$_E$ data, the best template fit identified by the *Euclid* pipeline is a K star, as depicted in orange in Fig. C2). The K star template closely matches the overall shape of the spectra, including the

Palomar/DBSP spectrum, which was not utilized for classification. However, this template fails to account for the broad emission lines observed in the NISP RG$_E$ spectrum at approximately 1200 and 1800 nm, which initially suggested a quasar classification. These prominent features, which are broader than the spectral resolution, are puzzling. Fortunately, this source is in the EDF-N, meaning that multiple epochs will be available to verify if the features in this spectrum are real.

[1]*Max-Planck-Institut für Astronomie, Königstuhl 17, D-69117 Heidelberg, Germany*

[2]*Aix-Marseille Université, CNRS, CNES, Laboratoire d'Astrophysique de Marseille, F-13388 Marseille, France*

[3]*INAF-Osservatorio di Astrofisica e Scienza dello Spazio di Bologna, Via Piero Gobetti 93/3, I-40129 Bologna, Italy*

[4]*Jet Propulsion Laboratory, California Institute of Technology, 4800 Oak Grove Drive, Pasadena, CA 91109, USA*

[5]*Astrophysics Group, Blackett Laboratory, Imperial College London, London SW7 2AZ, UK*

[6]*Department of Mathematics, Imperial College London, London SW7 2AZ, UK*

[7]*Instituto de Astrofísica e Ciências do Espaço, Universidade do Porto, CAUP, Rua das Estrelas, PT4150-762 Porto, Portugal*

[8]*DTx–Digital Transformation CoLAB, Building 1, Azurém Campus, University of Minho, P-4800-058 Guimarães, Portugal*

[9]*INAF-Osservatorio Astrofisico di Torino, Via Osservatorio 20, I-10025 Pino Torinese (TO), Italy*

[10]*Department of Physics, Astronomy and Mathematics, University of Hertfordshire, College Lane, Hatfield AL10 9AB, UK*

[11]*School of Physics and Astronomy, University of Leicester, University Road, Leicester, LE1 7RH, UK*

[12]*Departamento Física Aplicada, Universidad Politécnica de Cartagena, Campus Muralla del Mar, E-30202 Cartagena, Murcia, Spain*

[13]*International Space University, 1 rue Jean-Dominique Cassini, F-67400 Illkirch-Graffenstaden, France*

[14]*Université de Strasbourg, CNRS, Observatoire astronomique de Strasbourg, UMR 7550, F-67000 Strasbourg, France*

[15]*Instituto de Astrofísica de Canarias, Vía Láctea, E-38205 La Laguna, Tenerife, Spain*

[16]*Departamento de Astrofísica, Universidad de La Laguna, E-38206 La Laguna, Tenerife, FSpain*

[17]*Universite Marie et Louis Pasteur, CNRS, Observatoire des Sciences de l'Univers THETA Franche-Comte Bourgogne, Institut UTINAM, Observatoire de Besançon, BP 1615, F-25010 Besançon Cedex, France*

[18]*Université Claude Bernard Lyon 1, CNRS/IN2P3, IP2I Lyon, UMR 5822, F-69100 Villeurbanne, France*

[19]*INAF-Osservatorio Astrofisico di Arcetri, Largo E. Fermi 5, I-50125 Firenze, Italy*

[20]*Dipartimento di Fisica e Astronomia, Università di Firenze, via G. Sansone 1, I-50019 Sesto Fiorentino, Firenze, Italy*

[21]*Research Center for Space and Cosmic Evolution, Ehime University, 2-5 Bunkyo-cho, Matsuyama, Ehime 790-8577, Japan*

[22]*Department of Mathematics and Physics, Roma Tre University, Via della Vasca Navale 84, I-00146 Rome, Italy*

[23]*INAF-Osservatorio Astronomico di Roma, Via Frascati 33, I-00078 Monteporzio Catone, Italy*

[24]*Leiden Observatory, Leiden University, Einsteinweg 55, NL-2333 CC Leiden, the Netherlands*

[25]*Hamburger Sternwarte, University of Hamburg, Gojenbergsweg 112, D-21029 Hamburg, Germany*

[26]*Department of Astronomy, University of Massachusetts, Amherst, MA 01003, USA*

[27]*Max Planck Institute for Extraterrestrial Physics, Giessenbachstr. 1, D-85748 Garching, Germany*

[28]*Universitäts-Sternwarte München, Fakultät für Physik, Ludwig-Maximilians-Universität München, Scheinerstrasse 1, D-81679 München, Germany*

[29]*Dipartimento di Fisica e Astronomia 'Augusto Righi' – Alma Mater Studiorum Università di Bologna, via Piero Gobetti 93/2, I-40129 Bologna, Italy*

[30]*INAF-IASF Milano, Via Alfonso Corti 12, I-20133 Milano, Italy*

[31]*INAF-Osservatorio Astronomico di Padova, Via dell'Osservatorio 5, I-35122 Padova, Italy*

[32]*INFN-Padova, Via Marzolo 8, I-35131 Padova, Italy*

[33]*Aix-Marseille Université, CNRS/IN2P3, CPPM, F-13007 Marseille, France*

[34]*Dipartimento di Fisica e Astronomia 'G. Galilei', Università di Padova, Via Marzolo 8, I-35131 Padova, Italy*

[35]*Université Paris-Saclay, Université Paris Cité, CEA, CNRS, AIM, F-91191 Gif-sur-Yvette, France*

[36]*Technical University of Munich, TUM School of Natural Sciences, Physics Department, James-Franck-Str. 1, D-85748 Garching, Germany*

[37]*Max-Planck-Institut für Astrophysik, Karl-Schwarzschild-Str 1, D-85748 Garching, Germany*

[38]*Institut d'Astrophysique de Paris, UMR 7095, CNRS, and Sorbonne Université, 98 bis boulevard Arago, F-75014 Paris, France*

[39]*Centro de Astrobiología (CAB), CSIC-INTA, ESAC Campus, Camino Bajo del Castillo s/n, E-28692 Villanueva de la Cañada, Madrid, Spain*

[40]*Jodrell Bank Centre for Astrophysics, Department of Physics and Astronomy, University of Manchester, Oxford Road, Manchester M13 9PL, UK*

[41]*Instituto de Astrofísica de Canarias (IAC), Departamento de Astrofísica, Universidad de La Laguna (ULL), E-38200 La Laguna, Tenerife, Spain*

[42]*Institut d'astrophysique spatiale, Université Paris-Saclay, CNRS, F-91405 Orsay, France*

[43]*Institute for Astronomy, University of Edinburgh, Royal Observatory, Blackford Hill, Edinburgh EH9 3HJ, UK*

[44]*School of Physics, HH Wills Physics Laboratory, University of Bristol, Tyndall Avenue, Bristol BS8 1TL, UK*

[45]*Kavli Institute for the Physics and Mathematics of the Universe (WPI), University of Tokyo, Kashiwa, Chiba 277-8583, Japan*

[46]*Center for Data-Driven Discovery, Kavli IPMU (WPI), UTIAS, The University of Tokyo, Kashiwa, Chiba 277-8583, Japan*

[47]*School of Physics & Astronomy, University of Southampton, Highfield Campus, Southampton SO17 1BJ, UK*

[48]*Institute of Space Sciences (ICE, CSIC), Campus UAB, Carrer de Can Magrans, s/n, E-08193 Barcelona, Spain*

[49]*INAF-Istituto di Astrofisica e Planetologia Spaziali, via del Fosso del Cavaliere, 100, I-00100 Roma, Italy*

[50]*ESAC/ESA, Camino Bajo del Castillo, s/n., Urb. Villafranca del Castillo, E-28692 Villanueva de la Cañada, Madrid, Spain*

[51]*School of Mathematics and Physics, University of Surrey, Guildford, Surrey GU2 7XH, UK*

[52]*INAF-Osservatorio Astronomico di Brera, Via Brera 28, I-20122 Milano, Italy*

[53]*IFPU, Institute for Fundamental Physics of the Universe, Via Beirut 2, I-34151 Trieste, Italy*

[54]*INAF-Osservatorio Astronomico di Trieste, Via G. B. Tiepolo 11, I-34143 Trieste, Italy*

[55]*INFN, Sezione di Trieste, Via Valerio 2, I-34127 Trieste TS, Italy*

[56]*SISSA, International School for Advanced Studies, Via Bonomea 265, I-34136 Trieste TS, Italy*

[57]*Dipartimento di Fisica e Astronomia, Università di Bologna, Via Gobetti 93/2, I-40129 Bologna, Italy*

[58]*INFN-Sezione di Bologna, Viale Berti Pichat 6/2, I-40127 Bologna, Italy*

[59]*Centre National d'Etudes Spatiales–Centre spatial de Toulouse, 18 avenue Edouard Belin, F-31401 Toulouse Cedex 9, France*

[60]*Space Science Data Center, Italian Space Agency, Via del Politecnico snc, I-00133 Roma, Italy*

[61]*Dipartimento di Fisica, Università di Genova, Via Dodecaneso 33, I-16146 Genova, Italy*

[62]*INFN-Sezione di Genova, Via Dodecaneso 33, I-16146 Genova, Italy*

[63]*Department of Physics 'E. Pancini', University Federico II, Via Cinthia 6, I-80126 Napoli, Italy*

[64]*INAF-Osservatorio Astronomico di Capodimonte, Via Moiariello 16, I-80131 Napoli, Italy*

[65]*Faculdade de Ciências da Universidade do Porto, Rua do Campo de Alegre, P-4150-007 Porto, Portugal*

[66]*Dipartimento di Fisica, Università degli Studi di Torino, Via P. Giuria 1, I-10125 Torino, Italy*

[67]*INFN-Sezione di Torino, Via P. Giuria 1, I-10125 Torino, Italy*

[68]*Centro de Investigaciones Energéticas, Medioambientales y Tecnológicas (CIEMAT), Avenida Complutense 40, E-28040 Madrid, Spain*

[69]*Port d'Informació Científica, Campus UAB, C. Albareda s/n, E-08193 Bellaterra (Barcelona), Spain*

[70]*Institute for Theoretical Particle Physics and Cosmology (TTK), RWTH Aachen University, D-52056 Aachen, Germany*

[71]*INFN Section of Naples, Via Cinthia 6, I-80126, Napoli, Italy*

[72]*Dipartimento di Fisica e Astronomia 'Augusto Righi' – Alma Mater Studiorum Università di Bologna, Viale Berti Pichat 6/2, I-40127 Bologna, Italy*

[73]*European Space Agency/ESRIN, Largo Galileo Galilei 1, I-00044 Frascati, Roma, Italy*

[74]*Institute of Physics, Laboratory of Astrophysics, Ecole Polytechnique Fédérale de Lausanne (EPFL), Observatoire de Sauverny, CH-1290 Versoix, Switzerland*

[75]*Institut de Ciències del Cosmos (ICCUB), Universitat de Barcelona (IEEC-UB), Martí i Franquès 1, E-08028 Barcelona, Spain*

[76]*Institució Catalana de Recerca i Estudis Avançats (ICREA), Passeig de Lluís Companys 23, E-08010 Barcelona, Spain*

[77]*UCB Lyon 1, CNRS/IN2P3, IUF, IP2I Lyon, 4 rue Enrico Fermi, F-69622 Villeurbanne, France*

[78]*Mullard Space Science Laboratory, University College London, Holmbury St Mary, Dorking, Surrey RH5 6NT, UK*

[79]*Canada-France-Hawaii Telescope, 65-1238 Mamalahoa Hwy, Kamuela, HI 96743, USA*

[80]*Departamento de Física, Faculdade de Ciências, Universidade de Lisboa, Edifício C8, Campo Grande, PT1749-016 Lisboa, Portugal*

[81]*Instituto de Astrofísica e Ciências do Espaço, Faculdade de Ciências, Universidade de Lisboa, Campo Grande, P-1749-016 Lisboa, Portugal*

[82]*Department of Astronomy, University of Geneva, ch. d'Ecogia 16, CH-1290 Versoix, Switzerland*

[83]*Dipartimento di Fisica 'Aldo Pontremoli', Università degli Studi di Milano, Via Celoria 16, I-20133 Milano, Italy*

[84]*INFN-Sezione di Milano, Via Celoria 16, I-20133 Milano, Italy*

[85]*Institute of Theoretical Astrophysics, University of Oslo, P.O. Box 1029 Blindern, 0315 Oslo, Norway*

[86]*Department of Physics, Lancaster University, Lancaster LA1 4YB, UK*

[87]*Felix Hormuth Engineering, Goethestr 17, D-69181 Leimen, Germany*

[88]*Technical University of Denmark, Elektrovej 327, DK-2800 Kgs. Lyngby, Denmark*

[89]*Cosmic Dawn Center (DAWN), Denmark*

[90]*NASA Goddard Space Flight Center, Greenbelt, MD 20771, USA*

[91]*Department of Physics and Astronomy, University College London, Gower Street, London WC1E 6BT, UK*

[92]*Department of Physics and Helsinki Institute of Physics, Gustaf Hällströmin katu 2, FI-00014 University of Helsinki, Finland*

[93]*Département de Physique Théorique and Centre for Astroparticle Physics, Université de Genève, 24 quai Ernest-Ansermet, CH-1211 Genève 4, Switzerland*

[94]*Department of Physics, University of Helsinki, P.O. Box 64, FI-00014, Finland*

[95]*Helsinki Institute of Physics, Gustaf Hällströmin katu 2, University of Helsinki, FI-00014 Helsinki, Finland*

[96]*NOVA Optical Infrared Instrumentation Group at ASTRON, Oude Hoogeveensedijk 4, NL-7991PD, Dwingeloo, the Netherlands*

[97]*Centre de Calcul de l'IN2P3/CNRS, 21 Avenue Pierre de Coubertin, F-69627 Villeurbanne Cedex, France*

[98]*Argelander-Institut für Astronomie, Universität Bonn, Auf dem Hügel 71, D-53121 Bonn, Germany*

[99]*INFN-Sezione di Roma, Piazzale Aldo Moro, 2 - c/o Dipartimento di Fisica, Edificio G. Marconi, I-00185 Roma, Italy*

[100]*Department of Physics, Institute for Computational Cosmology, Durham University, South Road, Durham DH1 3LE, UK*

[101]*Astroparticule et Cosmologie, Université Paris Cité, CNRS, F-75013 Paris, France*

[102]*CNRS-UCB International Research Laboratory, Centre Pierre Binétruy, IRL2007, CPB-IN2P3, Berkeley, USA*

[103]*Institut d'Astrophysique de Paris, 98bis Boulevard Arago, F-75014 Paris, France*

[104]*Aurora Technology for European Space Agency (ESA), Camino bajo del Castillo, s/n, Urbanizacion Villafranca del Castillo, Villanueva de la Cañada, E-28692 Madrid, Spain*

[105]*Institut de Física d'Altes Energies (IFAE), The Barcelona Institute of Science and Technology, Campus UAB, E-08193 Bellaterra (Barcelona), Spain*

[106]*European Space Agency/ESTEC, Keplerlaan 1, NL-2201 AZ Noordwijk, the Netherlands*

[107]*School of Mathematics, Statistics and Physics, Newcastle University, Herschel Building, Newcastle-upon-Tyne, NE1 7RU, UK*

[108]*DARK, Niels Bohr Institute, University of Copenhagen, Jagtvej 155, DK-2200 Copenhagen, Denmark*

[109]*Waterloo Centre for Astrophysics, University of Waterloo, Waterloo, Ontario N2L 3G1, Canada*

[110]*Department of Physics and Astronomy, University of Waterloo, Waterloo, Ontario N2L 3G1, Canada*

[111]*Perimeter Institute for Theoretical Physics, Waterloo, Ontario N2L 2Y5, Canada*

[112]*Institute of Space Science, Str. Atomistilor, nr. 409 Măgurele, Ilfov 077125, Romania*

[113]*Consejo Superior de Investigaciones Cientificas, Calle Serrano 117, E-28006 Madrid, Spain*

[114]*Institut für Theoretische Physik, University of Heidelberg, Philosophenweg 16, D-69120 Heidelberg, Germany*

[115]*Institut de Recherche en Astrophysique et Planétologie (IRAP), Université de Toulouse, CNRS, UPS, CNES, 14 Av. Edouard Belin, F-31400 Toulouse, France*

[116]*Faculty of Sciences, Université St Joseph, Beirut, Lebanon*

[117]*Departamento de Física, FCFM, Universidad de Chile, Blanco Encalada 2008, Santiago, Chile*

[118]*Institut für Astro- und Teilchenphysik, Universität Innsbruck,, Technikerstr 25/8, A-6020 Innsbruck, Austria*

[119]*Institut d'Estudis Espacials de Catalunya (IEEC), Edifici RDIT, Campus UPC, E-08860 Castelldefels, Barcelona, Spain*

[120]*Satlantis, University Science Park, Sede Bld 48940, Leioa-Bilbao, Spain*

[121]*Infrared Processing and Analysis Center, California Institute of Technology, Pasadena, CA 91125, USA*

[122]*Instituto de Astrofísica e Ciências do Espaço, Faculdade de Ciências, Universidade de Lisboa, Tapada da Ajuda, P-1349-018 Lisboa, Portugal*

[123]*Niels Bohr Institute, University of Copenhagen, Jagtvej 128, DK-2200 Copenhagen, Denmark*

[124]*Departamento de Electrónica y Tecnología de Computadoras, Universidad Politécnica de Cartagena, Plaza del Hospital 1, E-30202 Cartagena, Spain*

[125]*INFN-Bologna, Via Irnerio 46, I-40126 Bologna, Italy*

[126]*Kapteyn Astronomical Institute, University of Groningen, PO Box 800, NL-9700 AV Groningen, the Netherlands*

[127]*INAF, Istituto di Radioastronomia, Via Piero Gobetti 101, I-40129 Bologna, Italy*

[128]*Department of Physics, Oxford University, Keble Road, Oxford OX1 3RH, UK*

[129]*ICL, Junia, Université Catholique de Lille, LITL, F-59000 Lille, France*

[130]*ICSC – Centro Nazionale di Ricerca in High Performance Computing, Big Data e Quantum Computing, Via Magnanelli 2, Bologna, Italy*

[131]*Department of Physics and Astronomy, University of British Columbia, Vancouver BC V6T 1Z1, Canada*

This paper has been typeset from a TEX/LATEX file prepared by the author.